Assessment of muscularis propria invasion in urothelial bladder carcinoma using continuous-time random walk and stretched-exponential models: Comparison with VI-RADS and apparent diffusion coefficient

YANGYING WU*, XIAOFANG ZHU*, XIAOLONG ZHOU, CANLI LIU, LI GUO, JINGANG HAO and YUNYUN SHANG

Department of Radiology, The Second Affiliated Hospital of Kunming Medical University, Kunming, Yunnan 650101, P.R. China

Received February 25, 2026; Accepted August 3, 2026

DOI: 10.3892/etm.2026.13316

Abstract. Accurate assessment of muscle layer invasion in bladder cancer is required to distinguish muscle-invasive bladder cancer (MIBC) from non-MIBC (NMIBC). The present prospective study evaluated continuous-time random-walk (CTRW) and stretched-exponential model (SEM) diffusion parameters against conventional apparent diffusion coefficient (ADC) and vesical imaging-reporting and data system (VI-RADS) scores. A total of 106 patients (62 MIBC and 44 NMIBC) who underwent 3.0T multiparametric magnetic resonance imaging, including multi-b-value diffusion-weighted imaging, at The Second Affiliated Hospital of Kunming Medical University (Kunming, China) were analyzed. CTRW and SEM parameters were extracted, and VI-RADS scores were assigned. Significant differences were found between groups for VI-RADS ≥4, SEM-ADC, CTRW-α and CTRW-β (P<0.05). Multivariate logistic regression identified VI-RADS ≥4 and CTRW-β as independent predictors of muscle invasion. While VI-RADS alone achieved an area under the curve (AUC) of 0.85, the combined model incorporating SEM-ADC, CTRW-α and VI-RADS achieved the highest overall performance (AUC=0.91; 95% CI: 0.86-0.96), significantly outperforming VI-RADS alone (raw P=0.002, Bonferroni-corrected P=0.004). Additionally, diffusion kurtosis was positively correlated with invasion depth (r=0.62). These findings indicate that advanced diffusion parameters, particularly CTRW-α and SEM-ADC, effectively differentiate MIBC from NMIBC. When integrated with VI-RADS, they significantly enhance diagnostic accuracy compared with VI-RADS alone (AUC: 0.91 vs. 0.85; P=0.030). Decision curve analysis confirmed clinical utility, with the combined model providing a mean net benefit gain of 0.10 (95% CI: 0.06-0.14) across the clinically relevant threshold range, corresponding with 10 additional correct diagnoses per 100 patients. These quantitative diffusion metrics represent promising non-invasive biomarkers for guiding therapeutic decisions.

Introduction

Bladder cancer ranks as the ninth most common malignancy globally, exhibiting marked epidemiological burden particularly among men (1). A notable challenge in the management of bladder cancer is the accurate differentiation between muscle-invasive bladder cancer (MIBC) and non-MIBC (NMIBC), as this distinction has implications for treatment selection and prognosis (2). Although established approaches, such as the vesical imaging-reporting and data system (VI-RADS) based on multiparametric magnetic resonance imaging (mp-MRI), have demonstrated utility in assessing muscularis propria invasion (3), and emerging biomarkers, including urinary lactoferrin and immune gene signatures, provide additional prognostic information (4), limitations remain. In particular, conventional diffusion-weighted imaging (DWI)-derived metrics, such as the apparent diffusion coefficient (ADC), despite their clinical value, are constrained by relatively low spatial resolution, limited tumor specificity and challenges related to inter-scanner and inter-protocol standardization (5). Consequently, there remains a need for more refined, non-invasive imaging biomarkers to improve the assessment of muscle invasiveness. Advanced DWI

Correspondence to: Professor Yunyun Shang or Professor Xiaolong Zhou, Department of Radiology, The Second Affiliated Hospital of Kunming Medical University, 374 Dianmian Avenue, Kunming, Yunnan 650101, P.R. China
E-mail: mri2507@126.com
E-mail: 1540578043@qq.com

*Contributed equally

Abbreviations: CTRW, continuous-time random walk; SEM, stretched-exponential model; ADC, apparent diffusion coefficient; VI-RADS, vesical imaging-reporting and data system; MIBC, muscle-invasive bladder cancer; NMIBC, non-MIBC; DWI, diffusion-weighted imaging; DCE, dynamic contrast-enhanced; ROC, receiver operating characteristic

Key words: bladder cancer, apparent diffusion coefficient, vesical imaging-reporting and data system, stretched-exponential model, continuous-time random walk, VI-RADS

models, including continuous-time random walk (CTRW) and stretched-exponential model (SEM) that capture complex tissue microstructure beyond Gaussian diffusion, have exhibited diagnostic potential inother tumor types, including prostate, breast, renal and head-and-neck cancers (6-8), while their specific utility and diagnostic performance for evaluating muscle layer invasion in bladder cancer, particularly vs. VI-RADS and conventional ADC, have not yet been well assessed (9).

Accurate discrimination between MIBC and NMIBC is essential for guiding treatment strategies and predicting prognosis (10). Although conventional imaging biomarkers such as DWI-derived ADC and VIRADS provide clinically useful information, their diagnostic utility is constrained by suboptimal spatial resolution, limited tumor specificity and inter-scanner/inter-protocol variability that compromise reproducibility (11,12). Advanced non-Gaussian diffusion models, such as the CTRW and SEM, have exhibited promise in other tumor types, including prostate, breast, renal and head-and-neck cancer (6-8), while their specific utility lies in the ability to capture complex microstructural heterogeneity of tissues via two parameters: α reflecting temporal diffusion heterogeneity and β reflecting spatial diffusion heterogeneity. However, their specific role in evaluating muscularis propria invasion in bladder cancer remains inadequately investigated (13).

Against this background, a more refined, non-invasive quantitative imaging approach is required to improve the assessment of muscle invasion.

MRI, particularly DWI and its quantitative parameter, the ADC, has become an area of active investigation in the diagnosis and staging of bladder cancer. DWI provides important information on tumor microenvironmental alterations by characterizing the diffusion behavior of water molecules in tissues. Numerous studies have demonstrated that ADC values possess notable predictive value for assessing muscularis propria invasion in bladder cancer (14,15). DWI has exhibited notable performance in bladder cancer staging and grading. Comparative analyses of single-parameter, dual-parameter and extended diffusion models have revealed marked differences in their ability to discriminate tumor stage and grade, particularly differences in ADC values between NMIBC and MIBC. Consequently, the combined application of DWI and ADC measurements provides valuable diagnostic and pathological classification information, including the differentiation of benign lesions from malignant bladder lesions (15). Despite these advantages, DWI is subject to several limitations, which include relatively low spatial resolution, limited tumor specificity and a lack of standardization in image acquisition protocols and post-processing methodologies, collectively restricting its clinical applicability and compromising the reproducibility of ADC measurements (16). The mp-MRI and biparametric MRI approaches have demonstrated improved diagnostic performance for predicting muscle layer invasion in bladder cancer, particularly when integrated with the VI-RADS framework (17,18). Beyond staging, DWI also exhibits potential in assessing tumor biological behavior. Specifically, ADC values have been proposed as imaging biomarkers of clinical aggressiveness, enabling differentiation between high- and low-grade tumors, as well as early- and advanced-stage disease (19). Furthermore, in patients with MIBC, combined DWI and ADC analysis has exhibited to promote the evaluation of response to neoadjuvant chemotherapy, contributing to improved long-term clinical outcomes (20).

Compared with conventional ADC, multi-b-value DWI models provide improved characterization of complex tissue heterogeneity. Advanced non-Gaussian diffusion models, such as intravoxel incoherent motion (IVIM) and diffusion kurtosis imaging (DKI), have demonstrated notable diagnostic utility in other malignancies, involving distinguishing histological grades in renal cell carcinoma (6), predicting distant metastasis in head and neck cancer (7) and characterizing orbital lesions (21). Similarly, advanced non-Gaussian diffusion models, including CTRW and SEM, are capable of characterizing complex diffusion behavior that reflects underlying tissue microstructural heterogeneity. Although advanced non-Gaussian diffusion models have demonstrated preliminary utility in bladder cancer grading (14), the diagnostic performance of CTRW- and SEM-derived parameters for assessing muscularis propria invasion, particularly their ability to discriminate MIBC from NMIBC and their comparative effectiveness relative to established standards, such as the VI-RADS and conventional ADC measurements, remains insufficiently investigated and has not been clearly established.

To address this knowledge gap, the present study systematically evaluated CTRW- and SEM-derived parameters for the assessment of MIBC and compared their diagnostic performance with that of conventional ADC and VI-RADS scores. Furthermore, by integrating multiple imaging-derived metrics and analytical approaches, the present study aimed to improve the accuracy of muscle invasion assessment and to provide more robust, non-invasive evidence to support clinical decision-making.

Therefore, the present study aimed to: (i) Determine whether CTRW and SEM-derived parameters can effectively discriminate MIBC from NMIBC; (ii) compare their diagnostic performance against conventional ADC and VIRADS; and (iii) assess whether multiparametric integration enhances diagnostic accuracy, thereby providing a robust, non-invasive imaging biomarker to support clinical decision-making.

Materials and methods

Patient enrollment. The present study was approved by the Ethics Committee of The Second Affiliated Hospital of Kunming Medical University (Kunming, China; approval no. 2024-217). A prospective case-control study was conducted on 106 patients diagnosed with bladder cancer between April 2025 and August 2025. According to the 2016 World Health Organization tumor classification system and the National Comprehensive Cancer Network clinical practice guidelines (22,23), patients were categorized into MIBC (62 cases) and NMIBC (44 cases) groups. Patient clinical and pathological data were collected, including age, sex, tumor stage and grade. Surgical procedures included transurethral resection of bladder tumor (TURBT) or radical cystectomy. The resected tissues or organs were sent for pathological examination. Inclusion criteria were as follows: i) Availability of complete clinical data; and ii) mp-MRI performed within 2 weeks prior to surgery. Exclusion criteria were as follows:

Table I. Detailed list of MRI scan parameters.

Name of sequence	B, sec/mm^2	Repetition time, msec	Echo time, msec	Deflection angle	Scan field, cm	Layer thickness, mm	Layer spacing, mm
Diffusion-weighted imaging	0, 50, 100, 150, 200 (1), 500 (2), 800 (2), 1,000 (4), 1,300 (4), 1,800 (6), 2,400 (8)	2,018	68.8	90˚	24x24	4	1
T2-weighted imaging	-	6,416	102.4	111˚	24x24	4	1
Dynamic contrast-enhanced	-	3.4	1.5	15˚	38x38	3	1.5

Numbers in parentheses in the b-value column indicate the number of signal averages acquired at each b-value.

i) Prior treatment before undergoing mp-MRI, including TURBT within 3 months, bladder biopsy within 2 weeks or cystoscopy within 3 days before imaging; ii) inadequate DWI quality; iii) tumor lesions <5 mm in maximum diameter, precluding reliable quantitative analysis; and iv) incomplete pathological information from TURBT (Fig. 1). Although the enrollment interval was relatively short (April-August 2025), all eligible patients presenting during this period were consecutively included. The Second Affiliated Hospital of Kunming Medical University maintains a stable, high-volume bladder cancer service, and no eligible cases were omitted, ensuring that the cohort reflects a representative clinical population. To preserve the representative nature of the sample and to minimize selection bias, uniform application of inclusion and exclusion criteria were used. The pathological reference standard was obtained from either TURBT or radical cystectomy specimens, depending on the definitive treatment received. For patients with NMIBC, complete TURBT specimens containing muscularis propria were used as the staging reference, whereas full-thickness radical cystectomy specimens served as the gold standard for patients with MIBC. To avoid the risk of understaging, cases with incomplete or indeterminate TURBT pathology were excluded according to the predefined criteria.

MRI acquisition. In the present study, all enrolled subjects underwent imaging examinations using the GE SIGNA Premier 3. 0T MRI scanner. The entire examination process strictly followed standardized protocols. Participants were instructed to empty their bladder 1 h prior to the examination and to ingest 500 ml of water in a standardized manner (a fixed volume consumed over a defined 30-min interval under consistent conditions) beginning 30 min prior to imaging to achieve adequate bladder distension. Once sufficient bladder distension was attained, the MRI sequences were acquired sequentially, including T1-weighted imaging (T1WI), T2-weighted imaging (T2WI), DWI and dynamic contrast-enhanced MRI (DCE-MRI).

The specific MRI acquisition protocols were as follows: Conventional T2WI was performed in the sagittal and axial planes, and fat-suppressed T2WI sequences were acquired in the coronal and axial planes. T1WI was obtained in the axial plane, including both non-fat-suppressed and fat-suppressed acquisitions. DWI was performed in the axial plane, with additional sagittal and coronal orientations. Axial DWI employed a multi-b-value acquisition, and ADC maps were generated through simultaneous image reconstruction. Contrast-enhanced imaging was carried out using gadopentetate dimeglumine administered at a dose of 0.2 ml/kg. Multiphase dynamic imaging was acquired using the liver acquisition with volume acceleration sequence, including axial arterial, venous and delayed phases, as well as sagittal and coronal equilibrium phases. In addition to multi-b-value DWI, DKI data were acquired using the same single-shot echo-planar imaging sequence with an extended high-b-value range to ensure stable higher-order diffusion modeling. Specifically, DKI reconstruction utilized b values of 0, 500, 1,000, 1,500, 2,000 and 2,400 sec/mm^2, consistent with established DKI acquisition practices (24). These b values were selected to optimize sensitivity to non-Gaussian diffusion behavior and to enable robust kurtosis estimation while maintaining acceptable signal-to-noise ratio. Detailed acquisition parameters for all MRI sequences are summarized in Table I.

Imaging examinations. In the present study, all enrolled subjects underwent imaging examinations using the GE SIGNA Premier 3. Patients were instructed to ingest 500 ml of water 30 min prior to imaging (as detailed in the MRI acquisition section) to achieve moderate bladder distension (target ~300 ml); in selected cases, up to 1,000 ml was permitted when adequate distension was otherwise not achieved. The imaging field of view involved the entire urinary bladder, proximal urethra and pelvic lymph nodes. The core MRI acquisition parameters were as follows. T1WI was performed using a spin-echo sequence [repetition time (TR)/echo time (TE)=600/11 msec; field of view (FOV)=240 mm; matrix=256x192; slice thickness=5 mm]. Axial T2WI was acquired with the following parameters: TR/TE=4,050/85 msec, FOV=200 mm, matrix=320x224 and slice thickness=6 mm. Fat-suppressed T2WI sequences were

obtained in the coronal (TR/TE=5,000/120 msec; FOV=220 mm) and sagittal (TR/TE=4,000/85 msec; FOV=300 mm) planes. DCE-MRI was performed using a three-dimensional gradient-echo sequence (TR/TE=3.9/1.4 msec; FOV=260 mm, matrix=192x192; slice thickness=3 mm) following intravenous administration of a gadolinium-based contrast agent at a dose of 0.1 mmol/kg and an injection rate of 1.5-2.0 ml/sec. A total of five to six dynamic phases were acquired over a temporal window of 20-131 sec. Multi-b-value DWI was performed using a single-shot echo-planar imaging sequence. The applied b values were 0, 50, 100, 150, 200, 500, 800, 1,000, 1,300, 1,800 and 2,400 sec/mm^2, with corresponding numbers of signal averages of 1, 1, 1, 1, 1, 2, 2, 4, 4, 6 and 8, respectively. The total DWI acquisition time was ~9 min. All imaging protocols were implemented in strict accordance with the VIRADS recommendations (25,26) to ensure reproducible assessment of muscularis propria invasion and pathological tumor grading.

Data analysis. DKI parameter estimation was performed using a standard diffusion kurtosis model to quantify non-Gaussian water diffusion. For each voxel, the diffusion-weighted signal S(b) was fitted to the second-order polynomial expression:
$S(b)=S_o \cdot \exp[-b \cdot D_{app} + (1/6)b^2 \cdot D_{app}^2 \cdot K_{app}]$, where D_{app} represents the apparent diffusion coefficient and K_{app} denotes the apparent kurtosis coefficient. Model fitting was performed using non-linear least-squares optimization across the dedicated DKI b values (0-2,400 sec/mm^2). Kurtosis maps were automatically generated by the iCare Spin workstation (Spin Imaging; Finnish company iCare, version 1.2.2), and mean K_{app} in each region-of-interest (ROI) was recorded as the representative DKI-kurtosis value.

The ADC value was calculated using the single exponential model formula $S=S_0 e^{-(DDC-b)\mu}$, where DDC denotes the distributed diffusion coefficient (equivalent to ADC under the mono-exponential model) and S and S0 are the signal strengths at b=800 and b=0 sec/mm^2, respectively. The CTRW model parameters (D, α and β) were fitted to multi-b-value diffusion data (b=0-3,000 sec/mm^2) using the Mittag-Leffler function-based signal model: $S(b)=S_0 \cdot E\_\alpha[-(bD)\text{^}\beta]$, where E_α denotes the Mittag-Lefler function of order α and D represents the anomalous diffusion coefficient, and α and β quantify the temporal and spatial heterogeneity of diffusion, respectively.

For the SEM, the parameters μ and distributed diffusion coefficient (DDC) were calculated using the stretched-exponential formulation. In addition, the SEM-kurtosis parameter was derived from a modified SEM model incorporating diffusion kurtosis effects. Signal decay was fitted according to the following equation: $S(b)=S_0 \cdot \exp[-(b \cdot DDC)^{\mu}+(1/6)b^2.DDC^2 \cdot K]$, where K denotes the SEM-kurtosis parameter, reflecting the degree of non-Gaussian diffusion.

Model parameters were extracted using non-linear least-squares fitting across multiple b values (0-2,400 sec/mm^2). The model fitting was performed using the iCare Spin workstation via the non-linear Levenberg-Marquardt algorithm with a subsection optimization strategy. Specifically, D was initially estimated using low b values (≤1,000 sec/mm^2), after which the fixed D values were used for global fitting of α and β (CTRW model) or μ and DDC (SEM model).

ROI delineation was independently performed by two experienced radiologists with 10 and 13 years of expertise in urological imaging. ROIs were manually drawn on the axial DWI images at the slice showing the maximum tumor diameter (b=800 sec/mm^2), with careful exclusion of necrotic or cystic areas. Diffusion parameter values for all pixels within each ROI were automatically extracted by the workstation, and the mean value of each parameter was calculated as the representative metric. The standard deviation and median were also recorded to characterize the dispersion and skewness of the parameter distributions.

To assess the reproducibility of quantitative diffusion parameters, interobserver agreement for ROI-based measurements between the two radiologists was evaluated using the intraclass correlation coefficient (ICC) based on a two-way random-effects model. Parameters with ICC values ≥0.75 were considered to demonstrate good reliability, and the averaged measurements from both readers were used in subsequent analyses.

VI-RADS scoring. A total of two experienced radiologists independently scored the cases using multi-parametric VI-RADS criteria, integrating comprehensive analysis of T2WI, DWI and DCE sequences (25). Both physicians had >1-year experience of diagnostic scoring, ensuring consistency in scoring standards. During the procedure, the physicians were blinded to clinical history and pathological results, and a 5-point scale score was assigned to each the bladder tumor from each patient. Scores ranged from 1 (definitely NMIBC) to 5 (definitely MIBC). Key observations included bladder wall layer disruption on T2WI, high signal diffusion restriction features on DWI and early enhancement patterns on DCE. In cases of initial discrepancies in image interpretation, consensus was achieved through joint image review and consultation of the VI-RADS decision tree, in which the highest assigned VI-RADS score was recorded as the final representative value. This process strictly adhered to multi-parametric integration principles, emphasizing the core value of DWI and DCE in differentiating T1/T2 staging. It was also validated that multi-parametric methods (mp-VI-RADS) could improve specificity and the area under the receiver operating characteristic (ROC) curve (AUC) for muscle invasion assessment compared with parametric approaches (for example bp-VI-RADS using only T2WI and DWI) (27). Interobserver agreement for VI-RADS scoring was quantified using Cohen's κ statistic. A κ>0.80 was interpreted as excellent agreement, 0.61-0.80 as good agreement and <0.60 as moderate or poor agreement. The final VI-RADS score used in the analysis was the consensus value reached after initial independent scoring.

Decision curve analysis (DCA). DCA was performed to evaluate the clinical utility of the predictive models by quantifying the net benefit across a range of threshold probabilities. Net benefit was calculated as: Net benefit=(True positives/N) - (False positives/N) x [P_t/(1 - P_t)], where N represents the total sample size (N=106), and P_t represents the threshold probability. The threshold probability represents the minimum predicted probability of muscle invasion at which a clinician would opt for radical cystectomy over bladder-preserving therapy. A total of four strategies were

compared: i) Treat-none (net benefit=0); i) treat-all (net benefit=prevalence - [1 - prevalence] x [P_t/(1 - P_t)]); iii) VI-RADS alone; and iv) the combined model (SEM-ADC + CTRW-α + VI-RADS). The clinically relevant threshold probability range was predefined as 20-80% based on clinical guidelines suggesting that patients with ≥20% predicted risk of muscle invasion should be considered for radical cystectomy, while thresholds >80% may lead to excessive overtreatment. DCA was conducted using the rmda package (version 1.6; https://cran.r-project.org/web/packages/rmda/) in R. The net benefit difference between the combined model and VI-RADS alone was calculated at 5% intervals within the clinically relevant range, and the mean net benefit difference was reported. Bootstrap resampling (n=1,000 iterations) was used to estimate 95% confidence intervals for the net benefit curves.

Statistical analysis. Statistical analysis was conducted using SPSS software (version [28.0]; IBM Corp.) for basic descriptive statistics and parametric comparisons, while R (version [4.2.1]; R Foundation for Statistical Computing) and Python (version [3.9.13]; Python Software Foundation) were employed for advanced modeling and machine learning tasks. Prior to parametric testing, the normality of distribution for all continuous variables was assessed using the Shapiro-Wilk test. The Shapiro-Wilk test revealed that age, mono-exponential ADC, SEM-ADC and CTRW-ADC followed normal distributions (all P>0.05), whereas CTRW-α, CTRW-β, SEM-kurtosis and DKI-kurtosis showed non-normal distributions (all P<0.05). Consequently, normally distributed continuous variables were compared between groups using Student's t-test or one-way analysis of variance, whereas non-normally distributed variables were analyzed using the Mann-Whitney U test. For pairwise comparisons following one-way analysis of variance, Tukey's honestly significant difference (HSD) post-hoc test was applied. Categorical variables were analyzed via the χ^2 test. Data are presented as mean ± standard deviation for normally distributed variables and median (interquartile range) for non-normally distributed variables. For non-normally distributed continuous variables that were included in multivariate logistic regression models, natural log transformation was applied to approximate normal distribution prior to model entry. The normality of transformed variables was confirmed using the Shapiro-Wilk test (all P>0.05 after transformation). Diagnostic performance of individual biomarkers and combined models was assessed using receiver operating characteristic (ROC) curve analysis, with the area under the curve (AUC) calculated using the trapezoidal rule. Pairwise comparisons of AUCs between different models were performed using DeLong's test for two correlated ROC curves. To control for Type I error inflation resulting from multiple pairwise comparisons, Bonferroni correction was applied by multiplying the raw P-values by the number of comparisons performed (m). Specifically, for comparisons involving k models, the total number of pairwise comparisons was m=k(k-1)/2. A corrected P<0.05 was considered to indicate a statistically significant difference. All ROC and DeLong's test analyses were conducted using the pROC package (version 1.18.0; https://cran.r-project.org/web/packages/pROC/) in R.

To identify effective predictive factors, univariate logistic regression was employed to screen variables with P<0.05, followed by multivariate analysis using stepwise regression and least absolute shrinkage and selection operator (LASSO) regularization to address multicollinearity and select the most significant features. For multi-parameter integration, principal component analysis (PCA) was applied to reduce dimensionality of multi-b-value DWI parameters, extracting principal components with cumulative variance contribution >85% to retain key information. The diagnostic performance of the multi-parameter model was evaluated using ROC curve analysis, with DeLong's test employed to compare the AUC between the multi-parameter model and the VI-RADS score. Calibration curves and DCA further validated the clinical utility and net benefit of the combined model. It should be noted that multivariate logistic regression was performed to identify independent statistical predictors, whereas the combined diagnostic model was developed using predictive-performance optimization. Because several diffusion parameters exhibited substantial inter-correlation, dimensionality-reduction (PCA) and regularization (LASSO) were applied to prevent multicollinearity and overfitting. These procedures consistently selected SEM-ADC and CTRW-α as the most informative quantitative predictors, even though CTRW-β remained statistically significant in the multivariate inferential model. Optimal cut-off values for all quantitative imaging parameters were determined using the Youden index (J=sensitivity + specificity-1) on the ROC curve. The corresponding thresholds reported for SEM-ADC, CTRW parameters, DKI kurtosis and mono-exponential ADC therefore represent the points that maximized the Youden index. For the VI-RADS score, the commonly used threshold of ≥4 (28,29) was also confirmed by the Youden index as the optimal discriminator between NMIBC and MIBC in the present cohort.

To minimize the risk of model overfitting, the events-per-variable (EPV) ratio was calculated for all regression models, and only variables achieving an EPV ≥10 were retained in the final multivariate analyses. Internal validation was performed using 1,000-bootstrap resampling with replacement to estimate optimism-corrected regression coefficients and calibration performance. The discriminative ability of each model was further corrected for optimism by computing the bias-adjusted AUC using bootstrap-based Harrell's method. For machine-learning models and LASSO feature selection, 10-fold cross-validation was applied to ensure model robustness and stability. All final reported AUC values, calibration curves and decision curve analyses were based on these internally validated, optimism-adjusted estimates.

Results

Clinical characteristics of participants. During data validation, the initially reported VI-RADS ≥4 distribution was found to be inconsistent with the logistic regression results. The results exhibited a higher proportion of VI-RADS ≥4 in the MIBC group, consistent with its role as a notable predictor of muscle invasion. No significant differences were identified between the two groups in terms of age (P=0.50) or sex (P=0.66); however, the VI-RADS score, which followed a non-normal distribution, was significantly higher in the MIBC

Table II. Comparison of clinical characteristics between the two groups of patients.

Feature	MIBC group (n=62)	NMIBC group (n=44)	Z/t/χ^2	P-value
Age, years	65.9±10.2	67.4±11.8	-0.68	0.500
Sex (male/female)	54/8	37/7	0.19	0.660
VIRADS score (median)	4 (3-5)	3 (2-4)	2.98	0.003
Proportion of VIRADS ≥4, % (n/total n)	61.3 (38/62)	20.5 (9/44)	14.22	<0.001
Tumor stage (T category), n (%)			106.05	<0.001
Ta	0 (0.0%)	26 (59.1%)		
T1	0 (0.0%)	18 (40.9%)		
T2	34 (54.8%)	0 (0.0%)		
T3	19 (30.6%)	0 (0.0%)		
T4	9 (14.5%)	0 (0.0%)		
Histological grade, n (%)			23.11	<0.001
Low grade (G1-G2)	9 (14.5%)	26 (59.1%)		
High grade (G3)	53 (85.5%)	18 (40.9%)		

MIBC, muscle-invasive bladder cancer; NMIBC, non-MIBC; VI-RADS, vesical imaging-reporting and data system.

group [4 (3-5)] compared with the NMIBC group [3 (2-4)] (P=0.003). The proportion of patients with VI-RADS ≥4 was 61.3% (38/62) in the MIBC group and 20.5% (9/44) in the NMIBC group (P<0.001). Interobserver reproducibility analyses revealed good to excellent reliability for ROI-based diffusion metrics (ICC=0.78-0.89). VI-RADS scoring demonstrated excellent agreement between the two radiologists, with a Cohen's κ value of 0.82. Detailed results are presented in Table II.

Comparison of DWI, CTRW, SEM parameters and VI-RADS between the NMIBC and MIBC groups. The DWI, CTRW and SEM parameters were compared between the two groups. For normally distributed variables, SEM-ADC was significantly lower in the MIBC group than in the NMIBC group (0.93±0.20 vs. 1.05±0.17; independent t-test, P=0.002). Similarly, CTRW-ADC (1.37±0.41 vs. 1.58±0.44; P=0.013) and DWI-ADC (1.69±0.44 vs. 1.88±0.41; P=0.026) were significantly lower in the MIBC group. For non-normally distributed variables analyzed using the Mann-Whitney U test, CTRW-α [median (IQR): 0.83 (0.72-0.94) vs. 0.95 (0.86-1.04); P<0.0001] and CTRW-β [0.93 (0.88-0.98) vs. 0.99 (0.96-1.02); P<0.0001] were significantly lower in the MIBC group. No significant difference was identified in SEM-kurtosis [0.71 (0.45-0.98) vs. 0.84 (0.62-1.06); P=0.362]. Detailed results are summarized in Table III.

Typical cases. An example patient was a 70-year-old woman diagnosed with high-grade papillary urothelial carcinoma. The tumor infiltrated the superficial muscular layer of the bladder wall, and no evidence of vascular or perineural invasion was identified. Carcinoma *in situ* lesions were present adjacent to the primary tumor. Another patient was a 65-year-old man with low-grade non-invasive papillary urothelial carcinoma, characterized by inverted growth, with no involvement of the muscularis propria. Representative color maps of the ROI and corresponding SEM- and CTRW-derived parameters (ADC and α) are illustrated on the original diffusion-weighted image (b=1,000 sec/mm^2). Compared with low-grade non-invasive papillary urothelial carcinoma, high-grade papillary urothelial carcinoma demonstrated lower mean diffusion parameter values (Figs. 2 and 3).

Independent predictive factors of muscle invasion. Univariate and multivariate logistic regression analyses were performed to evaluate the predictive value of multiparametric MRI parameters and clinical indicators for muscle invasion in bladder cancer. In the univariate logistic regression analysis, several variables were significantly associated with muscle-invasive disease, including SEM-ADC [P=0.001; odds ratio (OR)=0.05; 95% confidence interval (CI): 0.01-0.29], CTRW-α (P=0.002; OR=0.05; 95% CI: 0.01-0.32), CTRW-β (P=0.001; OR=0.01; 95% CI: 0.00-0.15), VI-RADS score (P=0.002; OR=6.35; 95% CI: 1.99-20.28) and VI-RADS ≥4 (P=0.001; OR=11.36; 95% CI: 2.61-49.46). Multivariate logistic regression analysis identified VI-RADS ≥4 (P=0.009; OR=6.49; 95% CI: 1.58-26.65) and CTRW-β (P=0.011; OR=0.04, 95% CI: 0.00-0.52) as independent predictors of MIBC. All included variables demonstrated VIF values between 1 and 5, indicating only mild multicollinearity and acceptable model stability. Detailed results are presented in Tables SI and SII.

Performance of multiple metrics for assessing muscle invasion. The diagnostic performance of individual biomarkers and combined models is summarized in Tables IV and SI-SIII. Among individual indicators, the VI-RADS score demonstrated the highest diagnostic performance, with an AUC of 0.85 (95% CI: 0.78-0.92), yielding a sensitivity of 82% and a specificity of 79% at a cut-off value of ≥4. CTRW-α_median (AUC=0.83; 95% CI: 0.75-0.90) and DKI-kurtosis (AUC=0.81; 95% CI: 0.73-0.89) exhibited slightly lower discriminative ability (Fig. 4). The mono-exponential ADC_mean exhibited the lowest diagnostic performance (AUC=0.78; 95% CI: 0.70-0.86). Pairwise

Table III. Comparison of DWI, CTRW, SEM parameters and VI-RADS between NMIBC and MIBC groups.

Parameter	MIBC group (n=62)	NMIBC group (n=44)	Mean difference (95% CI)	Statistical test	Test statistic	P-value
Normally distributed variables						
SEM-ADC	0.93±0.20 (0.88-0.98)	1.05±0.17 (1.00-1.10)	-0.12 (-0.19 - -0.05)	Independent t-test	t=-3.235	0.0020
CTRW-ADC	1.37±0.41 (1.27-1.47)	1.58±0.44 (1.45-1.71)	-0.21 (-0.38 - -0.04)	Independent t-test	t=-2.520	0.0130
DWI-ADC	1.69±0.44 (1.58-1.80)	1.88±0.41 (1.76-2.00)	-0.19 (-0.36 - -0.02)	Independent t-test	t=-2.252	0.0260
Non-normally distributed variables						
CTRW-α [median (IQR)]	0.83 (0.72-0.94)	0.95 (0.86-1.04)	-	Mann-Whitney U test	Z=-4.284	<0.0001
CTRW-β [median (IQR)]	0.93 (0.88-0.98)	0.99 (0.96-1.02)	-	Mann-Whitney U test	Z=-4.399	<0.0001
SEM-kurtosis [median (IQR)]	0.71 (0.45-0.98)	0.84 (0.62-1.06)	-	Mann-Whitney U test	Z=-0.915	0.3620

MIBC, muscle-invasive bladder cancer; NMIBC, non-MIBC; SEM, stretched-exponential model; CTRW, continuous-time random walk; ADC, apparent diffusion coefficient; DWI, diffusion-weight imaging.

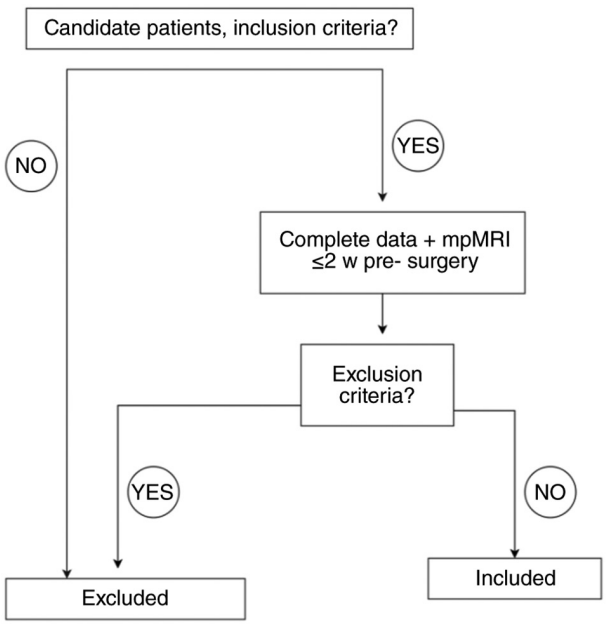

Figure 1. Patient selection process. A total of 106 patients with bladder cancer who underwent mp-MRI within 2 weeks prior to surgery were enrolled between April 2025 and August 2025. After applying the inclusion and exclusion criteria (prior treatment, inadequate diffusion-weighted imaging quality, lesion <5 mm and incomplete pathological data), the final cohort comprised 62 patients with MIBC and 44 with non-MIBC. mp-MRI, multiparametric magnetic resonance imaging; MIBC, muscle-invasive bladder cancer.

AUC comparisons using DeLong's test with Bonferroni correction for 15 comparisons (m=6x5/2) are presented in Table V. The combined model incorporating SEM-ADC, CTRW-α and VI-RADS achieved the highest overall performance (AUC=0.91; 95% CI: 0.86-0.96). This combined model significantly outperformed VI-RADS alone (raw P=0.002; Bonferroni-corrected P=0.030) and mono-exponential ADC_mean (raw P=0.001; Bonferroni-corrected P=0.015). Similarly, Combined Model 2 (DKI-kurtosis + SEM-ADC + CTRW-α, AUC=0.91; 95% CI: 0.85-0.96) significantly exceeded VI-RADS alone (raw P<0.001; Bonferroni-corrected P=0.006) and mono-exponential ADC_mean (raw P=0.001; Bonferroni-corrected P=0.015). No statistically significant difference was observed between Combined Model 1 and Combined Model 2 after Bonferroni correction (raw P=0.89; Bonferroni-corrected P>0.999) (Fig. 5). Comparative ROC analysis indicated that CTRW-α (AUC=0.83) was significantly superior to mono-exponential ADC (ΔAUC=0.05; raw P=0.03; Bonferroni-corrected P=0.450). Calibration plots demonstrated good agreement between predicted and observed MIBC probabilities for both combined models (Hosmer-Lemeshow test: Combined Model 1, χ^2=6.42, P=0.60; Combined Model 2, χ^2=7.15, P=0.52), indicating reliable probability estimates (Fig. S1).

DCA. Across the clinically relevant threshold probability range of 20-80%, the combined model consistently demonstrated positive net benefit and outperformed both the treat-all and treat-none strategies (Fig. 6A). The combined model achieved a maximum net benefit of 0.42 (95% CI: 0.31-0.53) at a threshold probability of 35%, compared with 0.34 (95% CI: 0.24-0.44) for VI-RADS alone at the same threshold (Table VI). Compared with VI-RADS alone, the combined model provided a mean net benefit difference of 0.10 (95% CI: 0.06-0.14) across the 20-80% threshold range, translating to ~10 additional correct diagnoses per 100 patients (range: 6-14) without increasing the rate of unnecessary interventions. The net benefit gain was most pronounced in the 25-50%

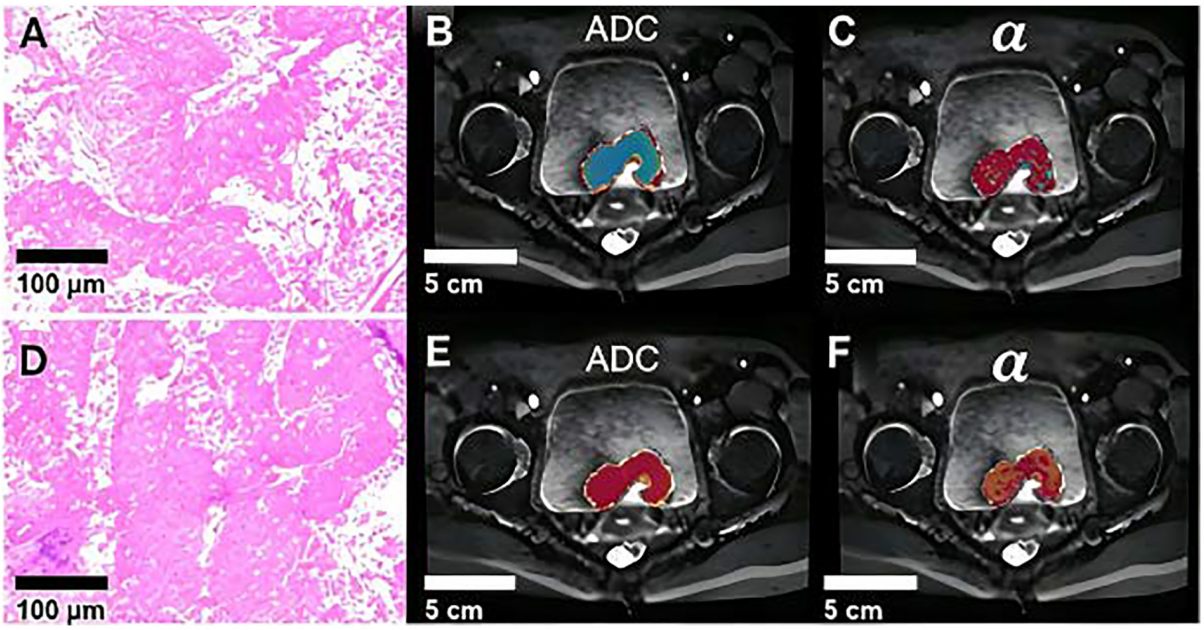

Figure 2. A 70-year-old female patient with high-grade papillary urothelial carcinoma. (A-F): (A) Microscopic pathological image, (B) pseudo-color image of CTRW-ADC, (C) CTRW-α, (D) microscopic pathological image, (E) pseudo-color image of SEM-ADC and (F) SEM-α. ADC, apparent diffusion coefficient; CTRW, continuous-time random walk; SEM, stretched-exponential model.

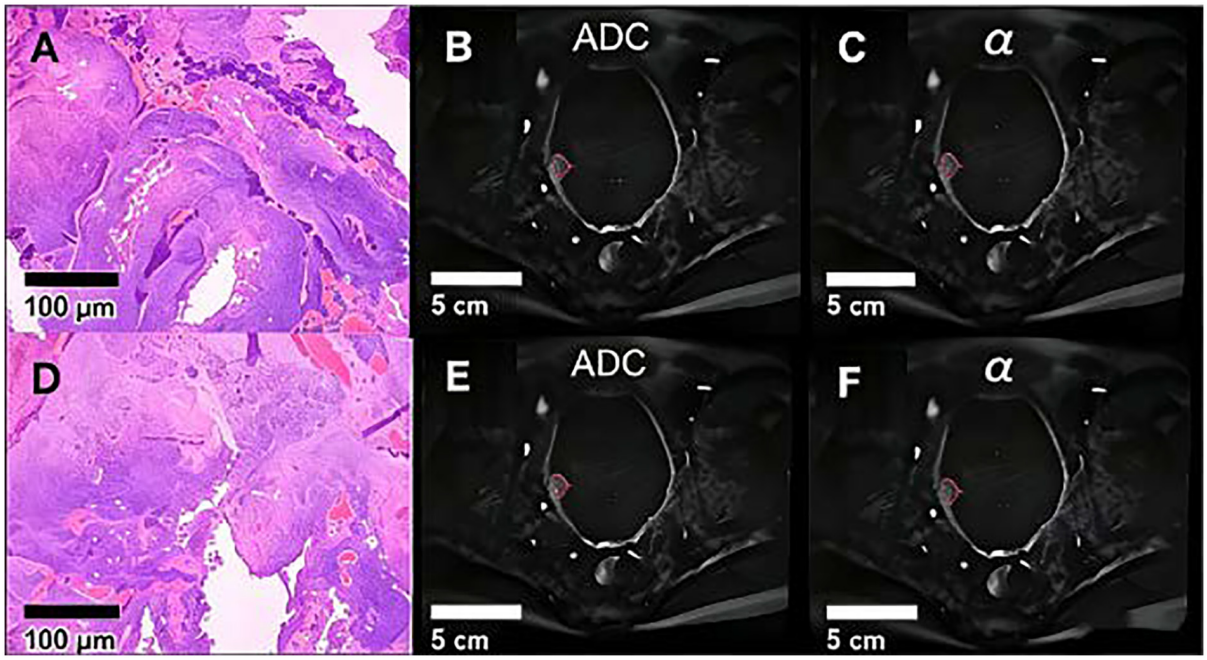

Figure 3. Low-grade non-invasive papillary urothelial carcinoma in a 65-year-old male patient. (A-F): (A) Microscopic pathological image, (B) pseudo-color image of CTRW-ADC, (C) CTRW-α, (D) microscopic pathological image, (E) pseudo-color image of SEM-ADC and (F) SEM-α. ADC, apparent diffusion coefficient; CTRW, continuous-time random walk; SEM, stretched-exponential model.

threshold range, where the combined model provided a net benefit difference of 0.12-0.15 compared with VI-RADS alone (Fig. 6B). At the predefined clinical threshold of 20%, the net benefit was 0.38 for the combined model vs. 0.28 for VI-RADS alone (difference: 0.10). At the 50% threshold, the net benefit was 0.25 vs. 0.16 (difference: 0.09). The treat-all strategy yielded negative net benefit below 62% threshold probability, while the treat-none strategy yielded zero net benefit across all thresholds (Table VI).

Discussion

The present study demonstrated that quantitative parameters derived from the CTRW anomalous diffusion exponent (α) and the SEM-ADC could significantly enhance the differentiation between MIBC and NMIBC. When integrated with the VI-RADS score, these parameters achieved a diagnostic AUC of 0.91, exceeding the performance of VI-RADS alone, as well as that of the conventional mono-exponential

Table IV. Summary of diagnostic performance.

Model/biomarker	AUC	95% CI	Sensitivity (%)	Specificity (%)	Cut-off
Individual biomarkers					
VI-RADS score	0.85	0.78-0.92	82	79	≥4
CTRW-α_median	0.83	0.75-0.90	81	77	0.89
DKI-kurtosis	0.81	0.73-0.89	76	81	0.68
Mono-exponential ADC_mean	0.78	0.70-0.86	74	73	$1.05x10^{-3}$ mm^2/sec
CTRW-α_mean	0.83	0.81-0.88	-	-	-
Combined models					
Combined Model 1 (SEM-ADC + CTRW-α + VI-RADS)	0.91	0.86-0.96	88	84	-
Combined Model 2 (DKI-kurtosis + SEM-ADC + CTRW-α)	0.91	0.85-0.96	86	85	-

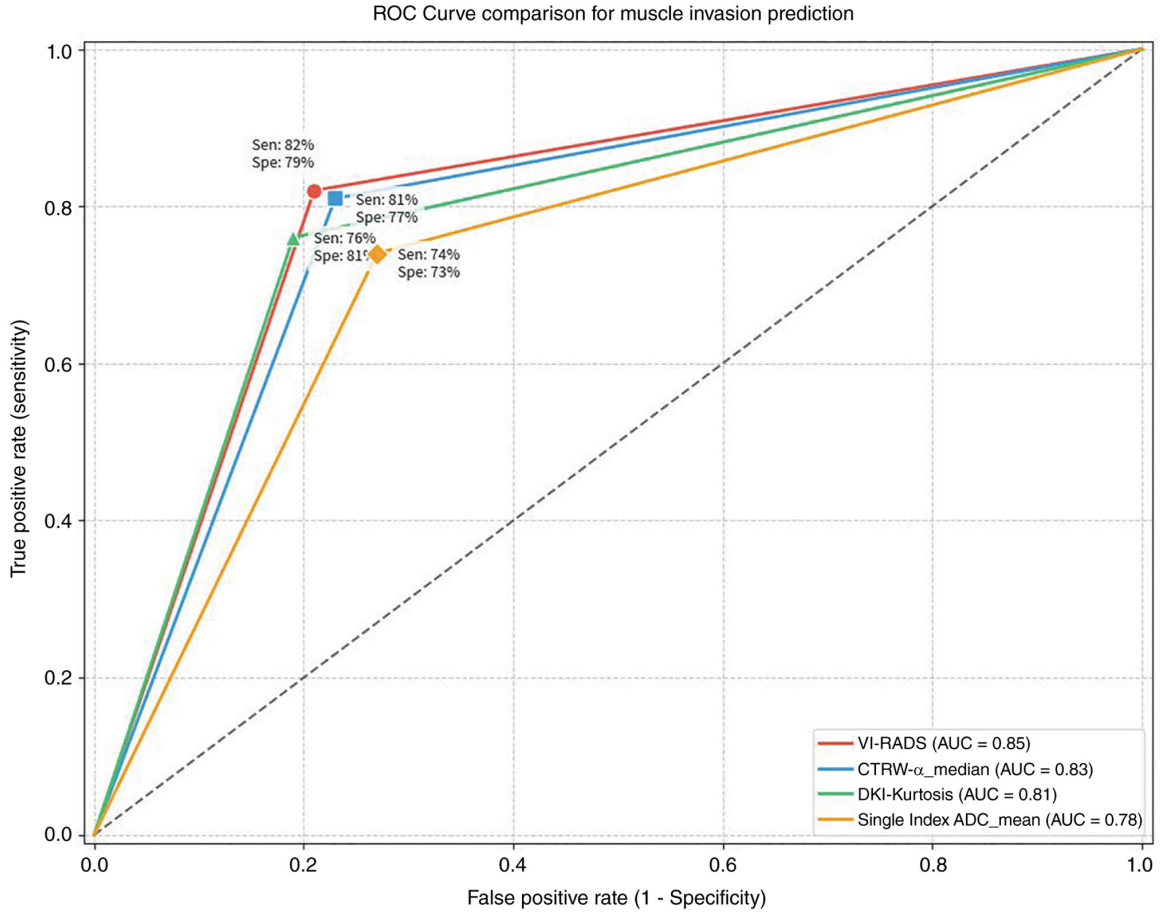

Figure 4. ROC analysis of imaging biomarkers for the diagnosis of muscle-invasive bladder cancer. Each curve represents the diagnostic performance of a single continuous parameter directly used as the test variable without transformation or model fitting: VI-RADS score (ordinal, 1-5), CTRW-α median (continuous, non-normally distributed), DKI-kurtosis (continuous, non-normally distributed), mono-exponential ADC mean (continuous, normally distributed), and CTRW-α mean (continuous, normally distributed). These curves represent the raw diagnostic information contained in each parameter individually. The x-axis (1-specificity) and y-axis (sensitivity) are derived by thresholding each parameter across its observed range. No statistical modeling, probability transformation or cross-validation is applied, as each parameter is evaluated in isolation. ROC, receiver operating characteristic; AUC, area under the curve; ADC, apparent diffusion coefficient; CTRW, continuous-time random walk; DKI, diffusion kurtosis imaging; Sen, sensitivity; Spe, specificity.

single-b-value ADC. These findings highlight the ability of multi-b-value diffusion models to capture intratumoral microstructural heterogeneity, supporting their potential role as non-invasive imaging biomarkers for clinical decision-making, including the selection between radical cystectomy and bladder-preserving treatment strategies. A methodological consideration in the present study is the comparison between conventional univariate ROC curves and multivariate

Table V. DeLong test pairwise comparison results matrix.

Comparison	ΔAUC	Raw P-value	Bonferroni-corrected P-value	Significant
Combined Model 1 vs. Mono-exp ADC	0.13	0.001	0.015	Yes
Combined Model 1 vs. VI-RADS	0.06	0.002	0.030	Yes
Combined Model 2 vs. Mono-exp ADC	0.13	0.001	0.015	Yes
Combined Model 2 vs. VI-RADS	0.06	<0.001	0.006	Yes
Combined Model 1 vs. DKI-kurtosis	0.10	0.003	0.045	Yes
Combined Model 2 vs. DKI-kurtosis	0.10	0.003	0.045	Yes
Combined Model 1 vs. CTRW-α_median	0.08	0.008	0.120	No
Combined Model 2 vs. CTRW-α_median	0.08	0.010	0.150	No
VI-RADS vs. Mono-exp ADC	0.07	0.012	0.180	No
CTRW-α_median vs. Mono-exp ADC	0.05	0.030	0.450	No
Combined Model 1 vs. CTRW-α_mean	0.08	0.025	0.375	No
Combined Model 2 vs. CTRW-α_mean	0.08	0.028	0.420	No
VI-RADS vs. DKI-kurtosis	0.04	0.120	1.000	No
CTRW-α_median vs. DKI-kurtosis	0.02	0.350	1.000	No
Combined Model 1 vs. Combined Model 2	0.00	0.890	1.000	No

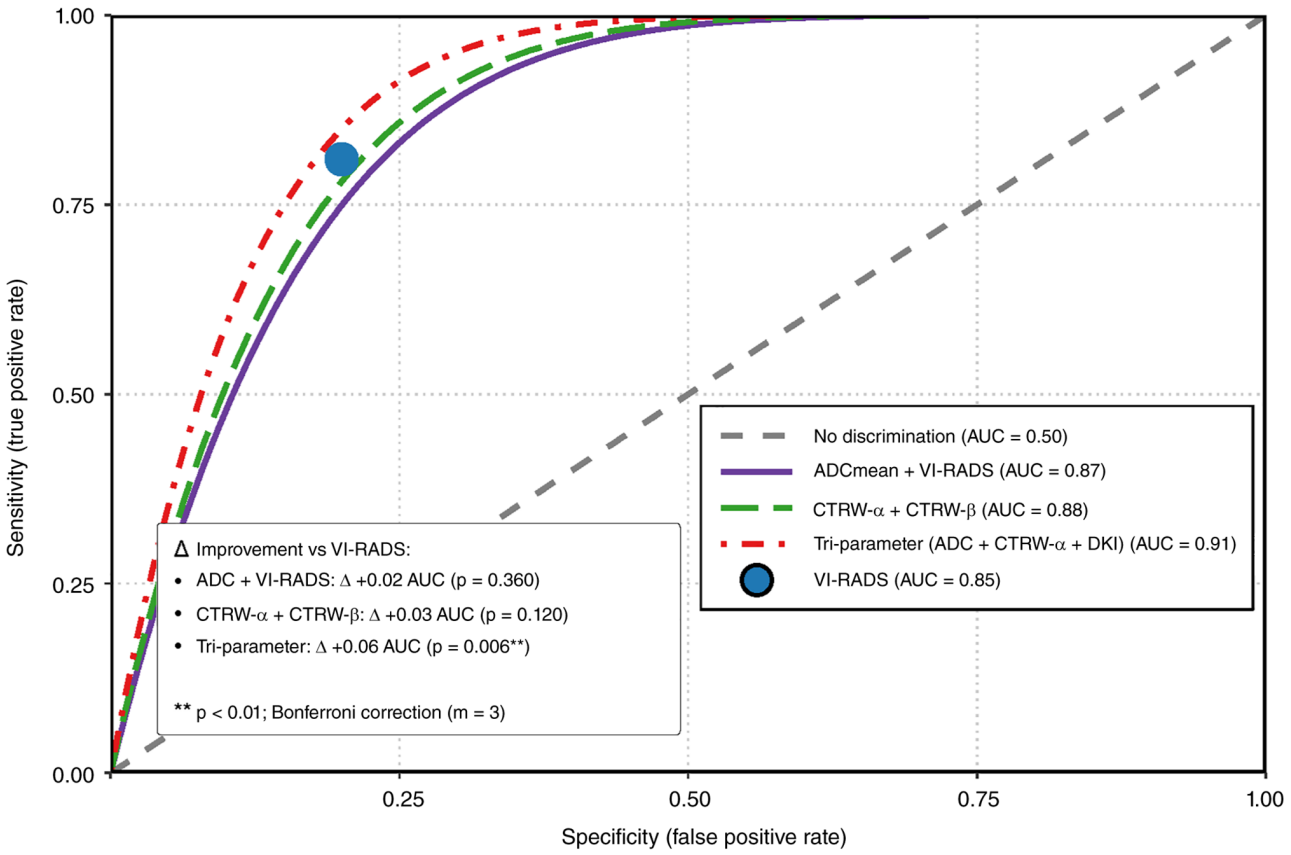

Figure 5. ROC analysis of combined multi-parametric models for the diagnosis of muscle-invasive bladder cancer. Shown are ROC curves for the combined models: ADCmean + VI-RADS (AUC=0.87, solid purple line), CTRW-α + CTRW-β (AUC=0.88, dashed green line), and the tri-parameter model (ADC + CTRW-α + DKI-kurtosis; AUC=0.91, dash-dot red line); the blue dot marks the optimal operating point of VI-RADS alone (AUC=0.85). The gray dashed diagonal line represents no discrimination (AUC=0.50). The inset lists the AUC improvement (Δ) of each combined model over VI-RADS alone, with pairwise P-values from DeLong tests under Bonferroni correction (m=3). ROC, receiver operating characteristic; AUC, area under the curve; ADC, apparent diffusion coefficient; CTRW, continuous-time random walk; DKI, diffusion kurtosis imaging; VI-RADS, vesical imaging-reporting and data system.

model-based ROC curves. While these curves differ in their construction, raw parameter values vs. predicted probabilities, several safeguards were implemented to ensure statistical comparability. First, the use of 10-fold cross-validation for

Table VI. Summary of decision curve analysis results.

Threshold probability (%)	Combined model net benefit (95% CI)	VI-RADS alone net benefit (95% CI)	Treat-all net benefit	Treat-none net benefit	Net benefit difference (95% CI)
20	0.38 (0.28-0.48)	0.28 (0.18-0.38)	0.15	0	0.10 (0.04-0.16)
25	0.40 (0.30-0.50)	0.27 (0.17-0.37)	0.05	0	0.13 (0.07-0.19)
30	0.41 (0.31-0.51)	0.29 (0.19-0.39)	-0.05	0	0.12 (0.06-0.18)
35	0.42 (0.31-0.53)	0.34 (0.24-0.44)	-0.15	0	0.08 (0.02-0.14)
40	0.40 (0.29-0.51)	0.31 (0.21-0.41)	-0.25	0	0.09 (0.03-0.15)
45	0.35 (0.24-0.46)	0.26 (0.16-0.36)	-0.35	0	0.09 (0.03-0.15)
50	0.25 (0.14-0.36)	0.16 (0.06-0.26)	–0.45	0	0.09 (0.02-0.16)
55	0.18 (0.07-0.29)	0.10 (0.00-0.20)	-0.55	0	0.08 (0.01-0.15)
60	0.12 (0.02-0.22)	0.05 (-0.05-0.15)	-0.65	0	0.07 (0.00-0.14)
65	0.08 (-0.02-0.18)	0.02 (-0.08-0.12)	-0.75	0	0.06 (-0.02-0.14)
70	0.04 (-0.06-0.14)	-0.01 (-0.11-0.09)	-0.85	0	0.05 (-0.04-0.14)
75	0.01 (-0.09-0.11)	-0.03 (-0.13-0.07)	-0.95	0	0.04 (-0.05-0.13)
80	-0.02 (-0.12-0.08)	-0.05 (-0.15-0.05)	-1.05	0	0.03 (-0.06-0.12)
Mean (20-80%)	0.22 (0.15-0.29)	0.12 (0.05-0.19)	-	-	0.10 (0.06-0.14)

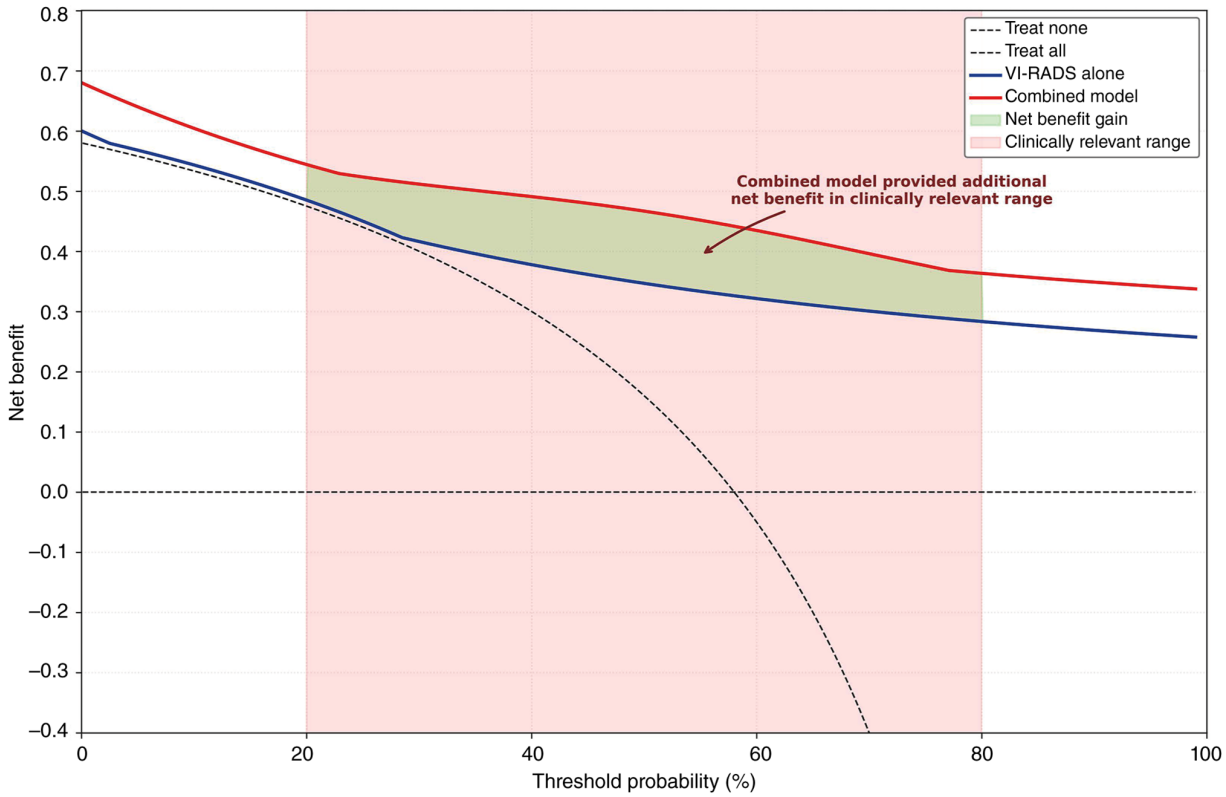

Figure 6. Decision curve analysis evaluating the clinical utility of predictive models for muscle-invasive bladder cancer. Net benefit curves for four clinical decision strategies across threshold probabilities from 0 to 100%: The combined model (SEM-ADC + CTRW-α + VI-RADS; solid blue line), VI-RADS alone (dashed red line), treat-all (dotted gray line), and treat-none (horizontal black line at net benefit=0). The shaded green area indicates the predefined clinically relevant threshold range (20-80%). The shaded orange area between the combined model and VI-RADS alone curves represents the net benefit gain achieved by the combined model. The combined model demonstrated superior net benefit across the entire clinically relevant range (20-80%), with a maximum net benefit of 0.42 at 35% threshold probability. At 20% threshold, the combined model yielded 0.38 vs. 0.28 for VI-RADS alone, corresponding to 10 additional correct diagnoses per 100 patients. ADC, apparent diffusion coefficient; CTRW, continuous-time random walk; SEM, stretched-exponential model; VI-RADS, vesical imaging-reporting and data system.

multivariate models mitigates overfitting, ensuring that Fig. 5 reflects out-of-sample performance rather than in-sample optimism. Second, it was demonstrated that univariate logistic regression predicted probabilities for VI-RADS yielded an identical AUC to conventional univariate ROC (0.85 vs. 0.85), confirming that the modeling framework per se does not

inflate diagnostic performance estimates. Third, calibration assessment validated that the predicted probabilities represent true probabilistic predictions. Fourth, supplementary metrics including NRI and IDI corroborated the AUC-based conclusions, providing evidence that the observed AUC improvement reflects genuine clinical reclassification rather than statistical artifact.

Compared with NMIBC, MIBC is characterized by notably lower ADC values, reflecting restricted water diffusion associated with increased cellular density and architectural complexity. ADC has exhibited to partially reflect tumor invasiveness and proliferative activity in bladder cancer. Previous research has reported notably lower ADC values in MIBC compared with NMIBC, being consistent with the higher cellular density and more aggressive biological behavior of muscle-invasive tumors (28). Furthermore, ADC values have been demonstrated to be negatively associated with the Ki-67 labeling index, supporting their association with tumor proliferative potential (30). However, despite its utility, the diagnostic performance of ADC alone in differentiating MIBC from NMIBC remains limited (31), and its independent predictive value for tumor recurrence has been reported to be suboptimal in some studies (31). Previous evidence demonstrated that combining ADC measurements with VI-RADS assessments derived from mp-MRI and bp-MRI (biparametric MRI) can improve diagnostic accuracy for muscle invasion (26). In particular, the integration of VI-RADS scores with ADC values has exhibited to markedly enhance diagnostic performance in the assessment of MIBC (32). Nevertheless, even with these combined approaches, ADC-based metrics alone generally provide only moderate discriminative ability in certain clinical settings, highlighting the added value of advanced non-Gaussian diffusion models, such as CTRW and SEM.

In the present study, CTRW-α and CTRW-β outperformed ADC in the detection of MIBC. The decrease in CTRW-α values is indicative of tissue disruption, whereas the reduction in CTRW-β values reflects diffusion abnormalities caused by microstructural chaos (8). The CTRW model exhibited marked diagnostic advantages in distinguishing benign lesions from malignant lesions. The CTRW model more effectively characterizes tissue microstructural alterations through variations in its α and β parameters, which is particularly relevant for the detection of MIBC, a disease characterized by marked structural complexity and heterogeneity (28,30). Conventional ADC measurements are subject to notable variability across MRI scanners, acquisition protocols and post-processing methods, thereby limiting their robustness and reliability as diagnostic biomarkers (33). Although multi-b-value diffusion techniques improve the stability of ADC estimation, they remain insufficient for fully characterizing diffusion behavior in biologically complex tissues. By contrast, the CTRW model explicitly incorporates both temporal and spatial aspects of anomalous diffusion, enabling a more comprehensive representation of non-Gaussian water diffusion in heterogeneous tumor microenvironments. By capturing subtle deviations from mono-exponential diffusion decay, the CTRW framework enhances sensitivity and specificity for detecting structurally complex lesions, such as MIBC, and provides a more biologically informative assessment of tumor invasiveness.

The SEM-ADC possesses notable advantages in discriminative capability, while the kurtosis parameter does not reach statistical significance, which has been validated and discussed in multiple studies. Previous research indicated that SEM-ADC more accurately reflects diffusion heterogeneity in biological tissues, whereas conventional mono-exponential ADC may underestimate such heterogeneity (34). SEM-ADC has demonstrated higher sensitivity and specificity across a range of tissue types, particularly in differentiating benign lesions from malignant lesions (35), reflecting notable clinical potential in applications requiring high-precision tissue characterization. Nevertheless, SEM-ADC remains limited in its ability to detect subtle microstructural abnormalities, especially when compared with the anomalous diffusion parameters (α and β) derived from the CTRW model. The CTRW framework has shown to more effectively capture microstructural abnormalities by characterizing non-Gaussian diffusion behavior, as supported by previous research (36). Although SEM-ADC provides a robust summary of overall diffusion characteristics, its sensitivity to fine-scale microstructural alterations is inferior to that of the CTRW α and β parameters (24). In this context, VIRADS ≥4 emerged as the strongest single predictor of MIBC (26,29), reflecting its value in standardized MRI interpretation. However, the reliance of VI-RADS on qualitative integration of T2WI, DWI, and DCE-MRI may contribute to false-positive assessments, particularly in the presence of inflammatory changes. Integrating VI-RADS ≥4 with quantitative diffusion metrics, including CTRW-β and tumor size, further improves diagnostic performance by reducing subjectivity and enhancing model robustness. Overall, multi-b-value diffusion models, such as CTRW and SEM, outperform conventional single-b-value ADC in the detection of MIBC. By sampling diffusion behavior across multiple b-values, these models capture non-Gaussian diffusion characteristics that are essential for accurately characterizing tumor complexity and heterogeneity.

The findings of the present study indicated that multi-parametric fusion (ADC + CTRW-α + VI-RADS) is advantageous in reducing false-negative results. By integrating multiple imaging parameters, the present study aimed to enhance diagnostic accuracy for bladder cancer, particularly in distinguishing NMIBC from MIBC. A prospective study confirmed that VI-RADS, as a standardized reporting method, achieved high clinical accuracy, with a sensitivity of 85.7% and a specificity of 86.9%, highlighting its notable clinical utility; however, the standalone use of VI-RADS has limitations, notably in terms of false-negative rates. Emerging evidence indicated that clinical factors, such as patient age and prostate-specific antigen density, which are not incorporated into the PI-RADSv2 algorithm, may contribute to false-negative diagnostic outcomes (36). Incorporation of complementary quantitative imaging parameters, including ADC and the CTRW-derived α parameter, provides a more comprehensive assessment of tissue microstructure and diffusion behavior, thereby mitigating the risk of false-negative findings. This multiparametric strategy integrates heterogeneous imaging features to enhance lesion characterization and

improve diagnostic sensitivity for malignant tissue detection (37). The clinical utility of the combined model was further supported by DCA, which demonstrated a mean net benefit gain of 0.10 across the clinically relevant threshold range (20-80%). This translates to ~10 additional correct diagnoses per 100 patients without increasing unnecessary interventions. The net benefit was most pronounced at threshold probabilities of 25-50%, which aligns with the clinical scenario where intermediate-risk patients pose the greatest diagnostic uncertainty. Notably, the treat-all strategy yielded negative net benefit <62% threshold, highlighting the substantial harm of overtreatment if all patients were subjected to radical cystectomy without risk stratification. Conversely, the treat-none strategy provided zero net benefit, underscoring the necessity of predictive modeling to identify candidates for aggressive therapy.

The present study has certain limitations that should be addressed. The present study was conducted at a single center, which might introduce inherent selection bias and limit the generalizability of the findings. The patient population, imaging protocols and clinical practices might not fully represent those of other institutions. While the multi-b-value protocol used in the present study possesses advantages in certain aspects of diffusion imaging, it requires longer acquisition time. Prolonged acquisition time increases the likelihood of involuntary motion during scanning, which in turn raises the risk of motion artifacts, potentially interfering with image quality and subsequent quantitative analysis. Therefore, future multi-center prospective studies with larger and more diverse cohorts are required to validate the robustness and external applicability of the present predictive model and imaging biomarkers.

In conclusion, the present study found that the α parameter derived from the CTRW model and the APC obtained from the SEM-ADC model could be effective in differentiating MIBC from NMIBC. Furthermore, integration of these quantitative diffusion parameters with the VI-RADS score, or their evaluation in comparison with VI-RADS alone, resulted in the improved diagnostic accuracy. These findings demonstrate that CTRW- and SEM-based diffusion metrics may serve as promising non-invasive imaging biomarkers to support the pathological stratification of bladder cancer.

Acknowledgements

Not applicable.

Funding

The present study was supported by the Yunnan Provincial Department of Education Fund Project (grant no. 2024J03480) and Yunnan Provincial Department of Science and Technology Kunming Medical University Joint Special Fund (grant no. 202401AY070001-337).

Availability of data and materials

The data generated in the present study may be requested from the corresponding author.

Authors' contributions

YS and XZhou were responsible for the research concept and design; YW and XZhu collected and/or assembled of data; CL, LG and JH performed the data analysis and interpretation; YW and XZhu wrote the article; YS and XZhou performed critical revision of the article. All authors have read and approved the final version of the manuscript. YS and XZhou confirm the authenticity of all the raw data.

Ethics approval and consent to participate

The present study was approved by the Ethics Committee of the Second Affiliated Hospital of Kunming Medical University (approval no. 2024-217), and written informed consent was obtained from all patients. The study was carried out in accordance with the Declaration of Helsinki and the Strengthening of the Reporting of Observational Studie in Epidemiology (STROBE) guidelines.

Patient consent for publication

Not applicable.

Competing interests

The authors declare that they have no competing interests.

References

1. Huang Q, Zhou Q, Zhang H, Liu Z, Zeng H, Chen Y, Qu Y, Xiong Y, Wang J, Chang Y, *et al*: Identification and validation of an excellent prognosis subtype of muscle-invasive bladder cancer patients with intratumoral CXCR5+ CD8+ T cell abundance. Oncoimmunology 9: 1810489, 2020.
2. Zangouei AS, Rahimi HR, Mojarrad M and Moghbeli M: Non coding RNAs as the critical factors in chemo resistance of bladder tumor cells. Diagn Pathol 15: 136, 2020.
3. Mir MC, Marchioni M, Zargar H, Zargar-Shoshtari K, Fairey AS, Mertens LS, Dinney CP, Krabbe LM, Cookson MS, Jacobsen NE, *et al*: Nomogram Predicting bladder cancer-specific mortality after neoadjuvant chemotherapy and radical cystectomy for muscle-invasive bladder cancer: Results of an International consortium. Eur Urol Focus 7: 1347-1354, 2021.
4. Drakaki A, Pantuck A, Mhatre SK, Dhillon PK, Davarpanah N, Degaonkar V, Surinach A, Chamie K and Grivas P: 'Real-world' outcomes and prognostic indicators among patients with high-risk muscle-invasive urothelial carcinoma. Urol Oncol 39: 76.e15-76.e22, 2021.
5. Matsumura E, Kosuge N, Nakanishi S, Suda T, Sugawa A, Fujimura T, Miyagi R, Yoshimi N and Saito S: Urine lactoferrin as a potential biomarker reflecting the degree of malignancy in urothelial carcinoma of the bladder. Tohoku J Exp Med 252: 225-244, 2020.
6. Cheng Q, Ren A, Xu X, Meng Z, Feng X, Pylypenko D, Dou W and Yu D: Application of DKI and IVIM imaging in evaluating histologic grades and clinical stages of clear cell renal cell carcinoma. Front Oncol 13: 1203922, 2023.
7. Fujima N, Sakashita T, Homma A, Yoshida D, Kudo K and Shirato H: Utility of a Hybrid IVIM-DKI model to predict the development of distant metastasis in head and neck squamous cell carcinoma patients. Magn Reson Med Sci 17: 21-27, 2018.
8. He L, Li F, Qin Y, Li Y, Hu Q, Liu Z, Zhang Y and Ai T: Enhanced preoperative prediction of breast lesion pathology, prognostic biomarkers, and molecular subtypes using multiple models diffusion-weighted MR imaging. Sci Rep 15: 4704, 2025.
9. Jin K, Qiu S, Jin D, Zhou X, Zheng X, Li J, Liao X, Yang L and Wei Q: Development of prognostic signature based on immune-related genes in muscle-invasive bladder cancer:bioinformatics analysis of TCGA database. Aging (Albany NY) 13: 1859-1871, 2021.

10. Li R, Naidu S, Fan W, Rose K, Huelster H, Grass GD, Vosoughi A, Dhillon J, Kim Y, Gupta S, *et al*: Effectiveness of perioperative chemotherapy and radical cystectomy in treating bladder cancer. Urol Oncol 41: 457.e17-457.e24, 2023.
11. Garneau CA, Marcotte N, Lacombe L, Fradet Y, Fradet V, Pouliot F, Toren P and Lodde M: Salvage therapy for BCG failure with intravesical sequential gemcitabine and docetaxel in patients with recurrent NMIBC. Can Urol Assoc J 18: 33-40, 2024.
12. Tan X, Liu Z, Cai T, Wang Y, Wu Z, Qin Z, Li Z, Liu Z, Yuan G, Zhou Q and Yao K: Prognostic significance of HER2 expression in patients with bacillus calmette-guérin-exposed non-muscle-invasive bladder cancer. Eur Urol Oncol 7: 760-769, 2024.
13. Kim SW, Yu H, Kim Y, Nam KH, Chae HK, Nam W, Eom DW, Park JY and Kim SJ: HER2 overexpression predicts pathological T2 stage and improved survival in de novo muscle-invasive bladder cancer after immediate radical cystectomy:a retrospective cohort study. Int J Surg 110: 847-858, 2024.
14. Wang Y, Hu D, Yu H, Shen Y, Tang H, Kamel IR and Li Z: Comparison of the diagnostic value of monoexponential, biexponential, and stretched exponential diffusion-weighted MRI in differentiating tumor stage and histological grade of bladder cancer. Acad Radiol 26: 239-246, 2019.
15. Dağgülli M, Onur MR, Fırdolaş F, Onur R, Kocakoç E and Orhan İ: Role of diffusion MRI and apparent diffusion coefficient measurement in the diagnosis, staging and pathological classification of bladder tumors. Urol Int 87: 346-352, 2011.
16. Lin WC and Chen JH: Pitfalls and limitations of diffusion-weighted magnetic resonance imaging in the diagnosis of urinary bladder cancer. Transl Oncol 8: 217-230, 2015.
17. Liu P, Cai L, Jiang L, Chen H, Cao Q, Bai K, Bai R, Wu Q, Yang X and Lu Q: Comparative diagnostic performance of VI-RADS based on biparametric and multiparametric MRI in predicting muscle invasion in bladder cancer. BMC Med Imaging 25: 60, 2025.
18. Kobayashi S, Koga F, Yoshida S, Masuda H, Ishii C, Tanaka H, Komai Y, Yokoyama M, Saito K, Fujii Y, *et al*: Diagnostic performance of diffusion-weighted magnetic resonance imaging in bladder cancer:potential utility of apparent diffusion coefficient values as a biomarker to predict clinical aggressiveness. Eur Radiol 21: 2178-2186, 2011.
19. Hafeez S, Koh M, Jones K, Ghzal AE, D'Arcy J, Kumar P, Khoo V, Lalondrelle S, McDonald F, Thompson A, *et al*: Diffusion-weighted MRI to determine response and long-term clinical outcomes in muscle-invasive bladder cancer following neoadjuvant chemotherapy. Front Oncol 12: 961393, 2022.
20. Xu S, Yao Q, Liu G, Jin D, Chen H, Xu J, Li Z and Wu G: Combining DWI radiomics features with transurethral resection promotes the differentiation between muscle-invasive bladder cancer and non-muscle-invasive bladder cancer. Eur Radiol 30: 1804-1812, 2020.
21. Lecler A, Duron L, Zmuda M, Zuber K, Bergès O, Putterman M, Savatovsky J and Fournier L: Intravoxel incoherent motion (IVIM) 3 T MRI for orbital lesion characterization. Eur Radiol 31: 14-23, 2021.
22. Bezhanova SD: Tumors of the kidney. The new 2016 WHO classification of tumors of the genitourinary system. Arkh Patol 79: 48-52, 2017 (In Russian).
23. Ettinger DS, Agulnik M, Cates JM, Cristea M, Denlinger CS, Eaton KD, Fidias PM, Gierada D, Gockerman JP, Handorf CR, *et al*: NCCN clinical practice guidelines occult primary. J Natl Compr Canc Netw 9: 1358-1395, 2011.
24. Wang P, Thapa D, Wu G, Sun Q, Cai H and Tuo F: A study on diffusion and kurtosis features of cervical cancer based on non-Gaussian diffusion weighted model. Magn Reson Imaging 47: 60-66, 2018.
25. Pecoraro M, Cipollari S, Messina E, Laschena L, Dehghanpour A, Borrelli A, Del Giudice F, Muglia VF, Vargas HA and Panebianco V: Multiparametric MRI for bladder cancer:A practical approach to the clinical application of VI-RADS. Radiology 314: e233459, 2025.
26. Wang Z, Shang Y, Luan T, Duan Y, Wang J, Wang H and Hao J: Evaluation of the value of the VI-RADS scoring system in assessing muscle infiltration by bladder cancer. Cancer Imaging 20: 26, 2020.
27. Zhang X, Wang Y, Xu X, Hu M, Wang S, Chen Y and Zhao X: Prospective comparison of 2D and 3D T2-weighted imaging in multiparametric MRI for assessing muscle invasion accuracy using VI-RADS in bladder cancer. Acad Radiol 31: 5034-5041, 2024.
28. Wang F, Wu LM, Hua XL, Zhao ZZ, Chen XX and Xu JR: Intravoxel incoherent motion diffusion-weighted imaging in assessing bladder cancer invasiveness and cell proliferation. J Magn Reson Imaging 47: 1054-1060, 2018.
29. Marchioni M, Primiceri G, Delli Pizzi A, Basilico R, Berardinelli F, Mincuzzi E, Castellucci R, Sessa B, Di Nicola M and Schips L: Could bladder multiparametric MRI be introduced in routine clinical practice? Role of the new VI-RADS score: Results from a prospective study. Clin Genitourin Cancer 18: 409-415.e1, 2020.
30. Kobayashi S, Koga F, Kajino K, Yoshita S, Ishii C, Tanaka H, Saito K, Masuda H, Fujii Y, Yamada T and Kihara K: Apparent diffusion coefficient value reflects invasive and proliferative potential of bladder cancer. J Magn Reson Imaging 39: 172-178, 2014.
31. Funatsu H, Imamura A, Takano H, Ueda T and Uno T: Can pretreatment ADC values predict recurrence of bladder cancer after transurethral resection? Eur J Radiol 81: 3115-3119, 2012.
32. Zhang Z, Xiao W, Wang Y, Zhang W and Luo M: Exploring the potential of the combined diagnostic model of ADC value and bp-MRI VI-RADS in the evaluation of muscle invasion in bladder cancer. Abdom Radiol (NY) 50: 3100-3107, 2025.
33. Alshuhri MS, Alhulail AA, Alqahtani AGM, Madkhali Y, Aljuhani M, Alghuraybi RA, Alqahtani S, Alomair OI, Alqahtani M, Qaisi AH and Almalki MS: Stability of ADC measurements in diffusion MRI:A multicenter phantom study using multi-point b-values. Radiography (Lond) 31: 212-219, 2025.
34. Park H, Kim SH, Lee Y and Son JH: Comparison of diagnostic performance between diffusion kurtosis imaging parameters and mono-exponential ADC for determination of clinically significant cancer in patients with prostate cancer. Abdom Radiol (NY) 45: 4235-4243, 2020.
35. Nakajo M, Fukukura Y, Hakamada H, Yoneyama T, Kamimura K, Nagano S, Nakajo M and Yoshiura T: Whole-tumor apparent diffusion coefficient (ADC) histogram analysis to differentiate benign peripheral neurogenic tumors from soft tissue sarcomas. J Magn Reson Imaging: Feb 22, 2018 (Epub ahead of print).
36. Mao C, Hu L, Jiang W, Qiu Y, Yang Z, Liu Y, Wang M, Wang D, Su Y, Lin J, *et al*: Discrimination between human epidermal growth factor receptor 2 (HER2)-low-expressing and HER2-overexpressing breast cancers:a comparative study of four MRI diffusion models. Eur Radiol 34: 2546-2559, 2024.
37. Salka B, Troost JP, Gaur S, Shankar PR, Diab AR, Hakim C, Mervak BM, Khalatbari S and Davenport MS: Clinical and imaging predictors of false-positive and false-negative results in prostate multiparametric MRI Using PI-RADS version 2. Radiol Imaging Cancer 7: e240019, 2025.